HOKKAIDO UNIVERSITY

Title	Catalysis of surface dispersed Cu2+ species on t-ZrO2: square-planar Cu catalyzed cross-coupling of arylboronic acid and imidazole
Author(s)	Kondo, Masaru; Joutsuka, Tatsuya; Fujiwara, Kakeru et al.
Citation	Catalysis science and technology, 13(7), 2247-2254 https://doi.org/10.1039/d3cy00024a
Issue Date	2023-04-07
Doc URL	https://hdl.handle.net/2115/91243
Type	journal article
File Information	CST 13(7)2247 .pdf

Hokkaido University Collection of Scholarly and Academic Papers : HUSCAP

Journal Name

ARTICLE

Catalysis of surface dispersed Cu^{2+} species on *t*-ZrO_2: Square-planar Cu catalyzed cross-coupling of arylboronic acid and imidazole

Received 00th January 20xx,
Accepted 00th January 20xx

DOI: 10.1039/x0xx00000x

www.rsc.org/

Masaru Kondo,*[a] Tatsuya Joutsuka,*[a,b] Kakeru Fujiwara,[c] Tetsuo Honma,[d] Masahiko Nishijima,[e] Shohei Tada*[f]

We examined the Chan-Lam cross-coupling of imidazole and arylboronic acids under additive-free and mild conditions using heterogeneous CuO/MO_x catalysts such as metal oxide-supported CuO and Cu-doped metal oxides. Among them, CuO/t-ZrO_2 exhibited the best performance, which was more than ten times the higher turnover number in comparison with bulk CuO. By combining experimental and computational approaches, we elucidated the surface structure of CuO/t-ZrO_2. The catalyst contained abundant highly reducible Cu^{2+} species, in contrast to the other Cu^{2+}-containing catalysts. Notably, X-ray absorption spectroscopy and density functional theory calculations revealed the Cu^{2+} species to be square-planar [CuO_4]. Our results indicate that the highly active [CuO_4] species play a key role in the present coupling reaction.

Introduction

Heterogeneous copper catalysts are attracting increasing attentions in both academia and industry owing to their unique catalytic activity, easy product separation, and low cost.[1] In the field of organic synthesis, they are applied in a variety of catalytic reactions such as oxidation, reduction, cross-coupling, and click reaction.[2] However, insoluble heterogeneous catalysts exhibit much lower catalytic activities than homogeneous catalysts. Therefore, heterogeneous copper-mediated catalysis often requires elevated temperature, high catalyst loadings, and chemical additives. Metal oxide–supported CuO catalysts have been utilized to improve their catalytic activity because they can easily control structures and electronic properties of the copper species.[2,3] Cu-doped metal oxide, which can modulate coordination modes, are also a robust catalyst.[4] Hence, we supposed that a highly reactive Cu species on the metal oxide surface would promote organic transformation under mild conditions. Herein, we focus on surface dispersed Cu^{2+} species on tetragonal zirconia.

Cu/ZrO_2 catalysts have been applied to hydrogenation and dehydrogenation.[5] Moreover, our group has reported the MeOH synthesis from carbon dioxide using a copper-doped zirconia catalyst precursor.[6] However, although crystal phases of ZrO_2, mainly monoclinic and tetragonal phases, have rarely been studied in organic synthesis, they are thought to have a crucial effect on the catalytic activity. In 2021, Hu et al. demonstrated that monoclinic ZrO_2-supported CuO (CuO/m-ZrO_2) exhibited superior performance in the hydrogenation of furfural and vanillin over Cu-doped tetragonal ZrO_2 (CuO/t-ZrO_2).[5f] In contrast, CuO/t-ZrO_2 was found to be a more suitable catalyst for their acetalization. Cu-catalyzed Chan-Lam coupling, a carbon-heteroatom bond formation reaction using boronic acids, is one of the most important transformations for the preparation of biologically active compounds and functional materials.[7] While a variety of homogeneous and heterogeneous Cu catalysts have been used for Chan-Lam coupling, CuO/ZrO_2 have never been explored. Thus, in this work, we demonstrate CuO/t-ZrO_2 catalyzed Chan-Lam coupling of arylboronic acids and imidazole under mild and additive-free conditions.[8] Moreover, the highly reactive Cu species and catalytic cycle of the present reaction were investigated by using both experimental and computational approaches.

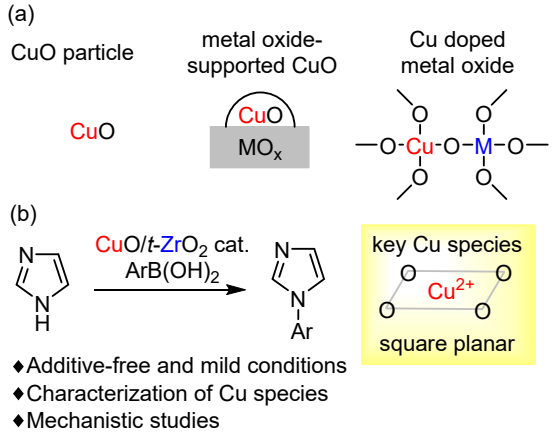

Fig. 1 (a) Heterogeneous Cu catalysts. (b) This work

[a] *Department of Materials Science and Engineering, Ibaraki University, Hitachi, Ibaraki 316-8511, Japan*
E-mail: masaru.kondo.fg74@vc.ibaraki.ac.jp, tatsuya.joutsuka.joe@vc.ibaraki.ac.jp
[b] *Frontier Research Center for Applied Atomic Sciences, Ibaraki University, Tokai, Ibaraki 319-1106, Japan*
[c] *Department of Chemistry and Chemical Engineering, Yamagata University, Yamagata 992-8510, Japan*
[d] *Japan Synchrotron Radiation Research Institute, Hyogo 679-5198, Japan*
[e] *Flexible 3D System Integration Lab, SANKEN, Osaka University, Mihogaoka, Ibaraki-shi, Osaka 567-0047, Japan*
[f] *Department of Applied Science and Engineering, School of Engineering, Hokkaido University, Kita 13, Nishi 8, Kita-ku, Sapporo, Hokkaido 060-8628, Japan*
E-mail: shohei.tada.st@eng.hokudai.ac.jp
Electronic Supplementary Information (ESI) available: CCDC 1973631.
DOI: 10.1039/x0xx00000x

Please do not adjust margins

Result and discussion

Catalyst performance

We commenced our study by screening catalysts for the Chan-Lam coupling of phenylboronic acid **1a** (0.2 mmol) and imidazole **2a** (0.2 mmol) in methanol and air at 50 °C for 8 h (entries 1–5, Table 1). When bulk CuO catalyst was used as the catalyst, the desired product **3a** was not formed (entry 1). When the CuO/TiO_2 catalyst was tested, **3a** was obtained in 23% yield (entry 2). The use of CuO/Al_2O_3 slightly improved the yield to 32% (entry 3), while Chan-Lam coupling catalyzed by CuO/*m*-ZrO_2 afforded **3a** in 42% yield (entry 4). Finally, CuO/*t*-ZrO_2 was determined to be the optimal catalyst for this transformation, affording **3a** in 81% yield (76% isolated yield, turnover number (TON) = 15, entry 5). This reaction did not proceed in THF and CH_3CN probably due to blocking of the copper coordination site (entries 6 and 7) and was significantly suppressed under argon atmosphere (20% yield, entry 8).

Table 1. Screening of catalysts and solvents[a]

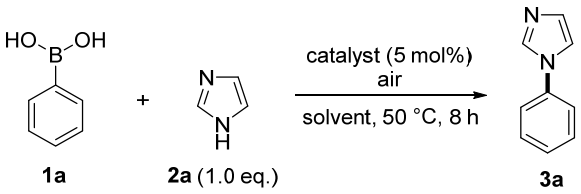

1a **2a** (1.0 eq.) **3a**

entry	catalyst	solvent	yield (%)[b]	TON
1	CuO	MeOH	<5	<1
2	CuO/TiO_2	MeOH	23	4.6
3	CuO/Al_2O_3	MeOH	32	6.4
4	CuO/*m*-ZrO_2	MeOH	42	8.2
5	CuO/*t*-ZrO_2	MeOH	81 (76)	16 (15)
6	CuO/*t*-ZrO_2	CH_3CN	<5	<1
7	CuO/*t*-ZrO_2	THF	<5	<1
8[c]	CuO/*t*-ZrO_2	MeOH	20	4

[a]Reaction conditions: **1a** (0.2 mmol), **2a** (0.2 mmol), Cu catalyst (0.01 mmol, 5 mol%) in solvent (1.0 mL, 0.2 M) at 50 °C in air. [b]1,3,5-Trimethoxybenzene was used as an internal standard. Isolated yield is shown in parentheses. [c]Under argon atmosphere.

Structural analysis by experiments

To consider the different activities of each Cu catalyst in Table 1, we analyzed surface Cu species. The CuO loading of the prepared catalysts was approximately 1 mmol g_{cat}^{-1}, as measured by XRF (Table S1, ESI). First, we examined the crystal structure of the as-prepared catalysts using XRD (Fig. 2). The XRD pattern of each catalyst presented peaks corresponding to its support. On the other hand, CuO peaks were either weak or absent, indicating that the CuO nanoparticles are smaller than the XRD detection limit (<10 nm) and/or that the Cu species are different from those in bulk CuO. In the latter case, they can be incorporated into the lattice of metal oxide supports. Fig. 3a shows the Cu-K-edge X-ray absorption near edge structure (XANES) spectra of the Cu-based catalysts. As references, data for CuO, Cu_2O, and Cu foil were also collected. The peak at ~8980 eV was attributed to the 1*s* → 4*pπ* transition, whereas that at ~8992 eV was attributed to the 1*s* → 4*pσ* transition.[9] For all the Cu-based catalysts except for CuO/*t*-ZrO_2, the XANES spectra were similar to those of CuO. For CuO/*t*-ZrO_2, the XANES spectrum displayed a white line characterized by double peaks at 8988 and 8993 eV ~~and no shoulder peak at 8980 eV~~. Thus, we supposed that the Cu species in CuO/*t*-ZrO_2 were different from those in CuO. Fig. 3b shows the Cu K-edge radial structure functions (RSFs). A strong backscattering peak at 1.5 Å was assigned to the nearest-neighbor Cu–O distance of 1.96 Å (see Table S2). The peak at 2.5 Å was assigned to the second-neighbor CuO, and first- and second-neighbor Cu–Cu coordinations. The fitting results revealed that CuO comprised distorted octahedral clusters [CuO_6]. For CuO/TiO_2 and CuO/*m*-ZrO_2, the RSF was similar to that of CuO. Therefore, we concluded that these samples contained CuO nanoparticles supported by the corresponding metal oxides. Both the XRD (Fig. 2) and RSF (Fig. 3b) indicate that the CuO nanoparticle size was <10 nm. In the case of CuO/Al_2O_3, the second peak at 2.5 Å was weak. Following fitting, we could only recognize the peak of the second-Cu–O coordination but not those of the first- and second-neighbor Cu–Cu coordinations (Table S2). This indicated the sample mainly contained isolated octahedral clusters [CuO_6]. Notably, for CuO/*t*-ZrO_2, the peak at 2.5 Å was not observed. The coordination number of Cu–O was 3.9±0.4, indicating that the Cu species in CuO/*t*-ZrO_2 was a four-fold coordinated Cu cluster [CuO_4]. As shown in Figs. S1 and S2, the RSF and XRD of the spent CuO/*t*-ZrO_2 were similar to that of the as-prepared CuO/*t*-ZrO_2, which confirms that the [CuO_4] species was present even after the reaction.

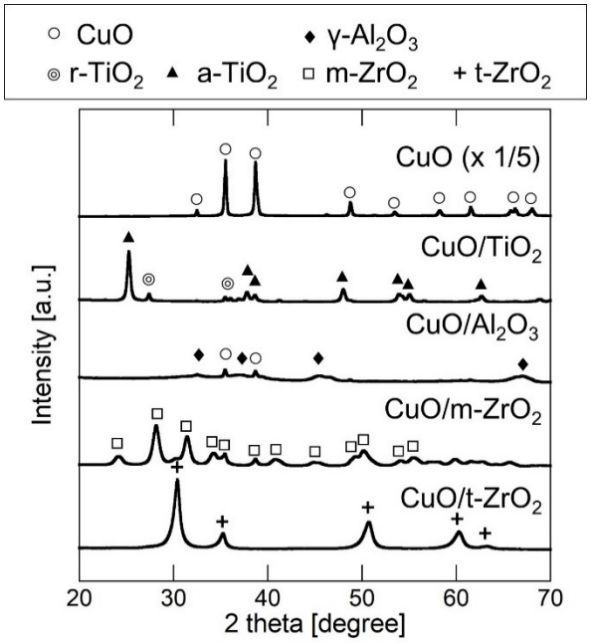

Fig. 2 XRD patterns of the prepared catalysts and CuO.

This journal is © The Royal Society of Chemistry 20xx

Please do not adjust margins

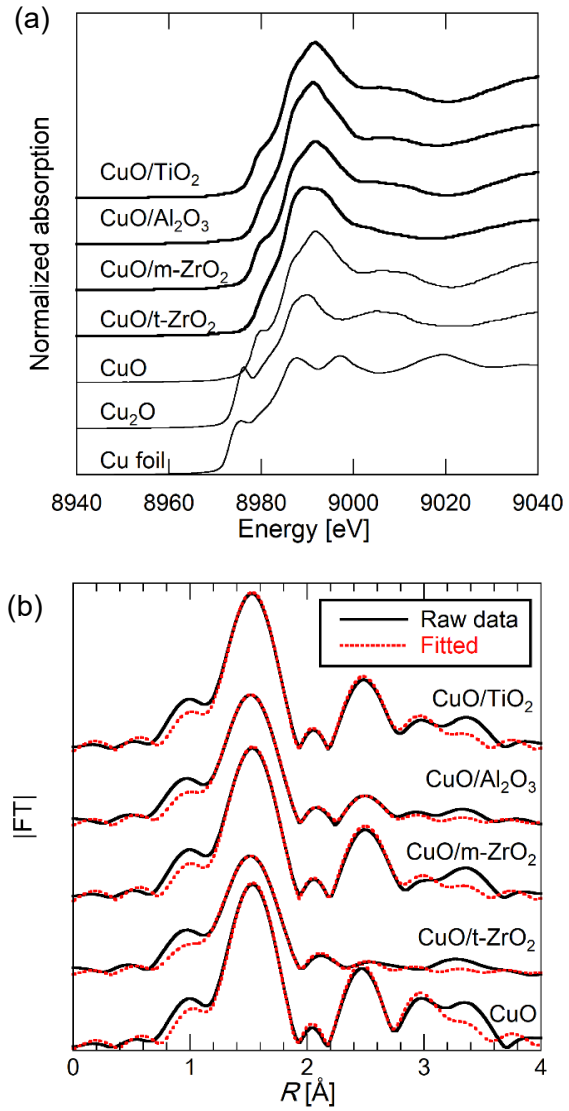

Fig. 3 (a) Cu-K edge XANES spectra of the Cu-based catalysts, CuO, Cu_2O, and Cu foil. (b) Fourier transforms of the k^3-weighted extended X-ray absorption fine structure (EXAFS) oscillations measured at room temperature near the Cu K-edge of the as-prepared catalysts, Cu foil, Cu_2O, and CuO; k range = 30-110 nm^{-1} and R range = 1.0-3.4 Å.

Fig. 4 shows high-angle annular dark field scanning transmission electron microscopy (HAADF-STEM) images of as-prepared CuO/*t*-ZrO_2. We can observe several particles with the size = ca. 10 nm. Each particle contained Zr and Cu species, according to the elemental mapping. Additionally, we checked the morphology of the spent CuO/*t*-ZrO_2. The catalyst was used for the above Chan-Lam coupling (Entry 5). Of note, only the nanoparticles containing Zr and Cu were seen in Fig. 4b, which means that Cu species are well-dispersed even after the reaction. Hence, the HAADF-STEM observation is in line with the results of Cu K-edge XAS (Figs. 3 and S1).

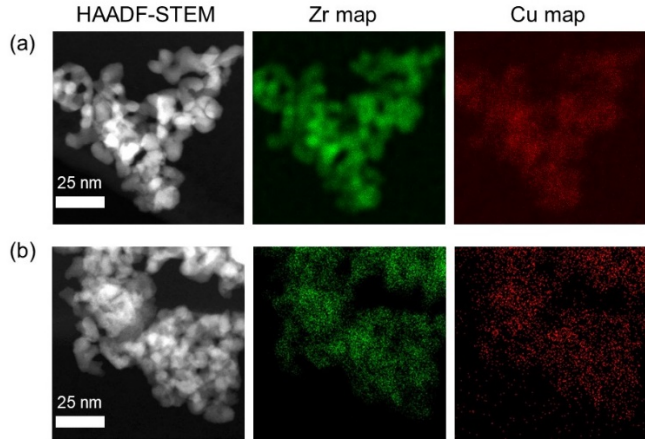

Fig. 4 HAADF-STEM images and elemental mapping of (a) as-prepared and (b) spent CuO/*t*-ZrO_2.

Thus, we determined that the types of MO_x determines the Cu coordination structure. We next proceeded to investigate whether reducibility of the Cu^{2+} species is related to the coordination structure. Such knowledge can be informative because the proposed reaction pathway of Cu-catalyzed Chan-Lam coupling is considered to include a redox cycle of the Cu species.[7] Thus, we performed H_2-TPR to analyze the reducibility of the Cu^{2+} species in the as-synthesized Cu-based catalysts. Fig. 5 shows the H_2-TPR profiles of CuO and the prepared catalysts. For CuO, the broad reduction peak at 250–400 °C indicated that the Cu^{2+} species in CuO was reduced by H_2 above 250 °C. For the Cu-based catalysts, the reduction peaks were observed below 250 °C. Hence, we supposed that the interaction between Cu and the metal oxides improves the reducibility of the Cu^{2+} species. Two peaks, namely a low-temperature and a high-temperature peak were observed for

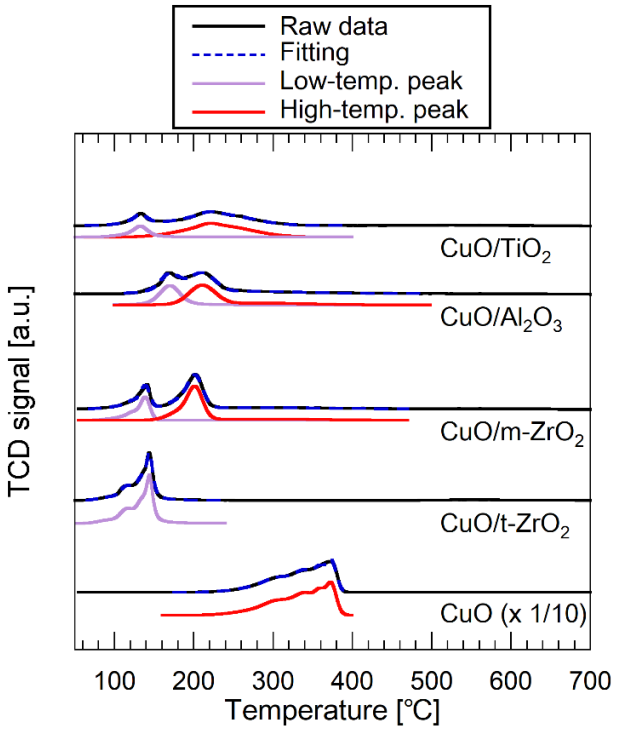

Fig. 5 H_2-TPR profiles of the Cu-based catalysts and CuO (reference).

Please do not adjust margins

Table 2. H_2 consumption in the H_2-TPR experiment.

sample	H_2 consumption [mmol g_{cat}^{-1}]		
	Low temp.[a]	High temp.[b]	Total
CuO/TiO_2	0.21	0.70	0.91
CuO/Al_2O_3	0.42	0.60	1.02
$CuO/m\text{-}ZrO_2$	0.30	0.68	0.98
$CuO/t\text{-}ZrO_2$	0.71	0	0.71

[a] Based on the low-temperature peak in Fig. 5. [b] Based on the high-temperature peak in Fig. 5.

$CuO/m\text{-}ZrO_2$, CuO/TiO_2, and CuO/Al_2O_3. Approximately 30% of the Cu^{2+} species were reduced below 150 °C, whereas the rest of the species were reduced at ~200 °C. Most of the Cu^{2+} species were expected to be reduced to metallic Cu by H_2 molecules below 500 °C because the total H_2 consumption was almost the same as the Cu loading (1 mmol g_{cat}^{-1}). For $CuO/t\text{-}ZrO_2$, only the peak below 150 °C was observed. Notably, according to Table 2, the H_2 consumption based on the corresponding peak area (0.71 mmol g_{cat}^{-1}) was smaller than that of the Cu loading (1 mmol g_{cat}^{-1}). This phenomenon was also predicted in our previous work.[6b] We then carried out XANES analysis of the H_2-reduced $CuO/t\text{-}ZrO_2$ based on the linear combination fitting. While 68% of the Cu^{2+} species were reduced to Cu^0, the remainder unchanged. These results indicated that ~70% of the Cu^{2+} species in $CuO/t\text{-}ZrO_2$ are highly reducible, while the others exist as ultra-stable Cu^{2+} species. Our previous hypothesis was in line with the present H_2-TPR results.

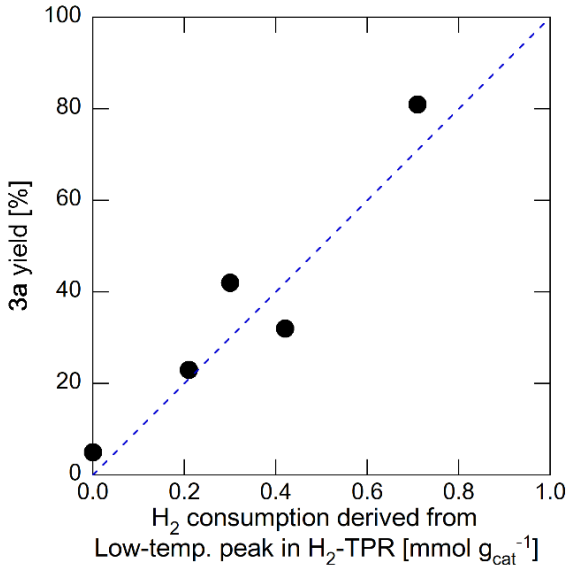

Fig. 6 Plots of the product (**3a**) yield against H_2 consumption calculated from the low-temperature H_2-TPR peaks.

Of note, we found the relationship between the product yield and Cu^{2+} reducibility. Fig. 6 shows the plots of the yield of **3a** against the H_2 consumption calculated from the low-temperature H_2-TPR peaks. These two values are positively correlated. As described above, the low-temperature peak is assignable to the reduction of highly reducible Cu^{2+} species. The peak area is related to the number of the Cu^{2+} species. Hence, we concluded that the highly reducible Cu^{2+} species are essential to Chan-Lam coupling.

Structural analysis using DFT calculations

We have experimentally revealed that the Cu^{2+} species in $CuO/t\text{-}ZrO_2$ are unique and essential for Cu-catalyzed Chan-Lam coupling. To gain molecular-level insight into the surface of $CuO/t\text{-}ZrO_2$, we next performed DFT calculations.

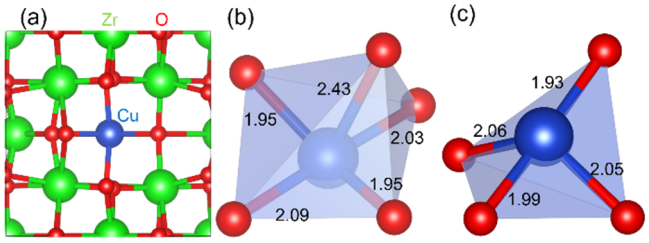

Fig. 7 Structures of (a) bulk $CuO/t\text{-}ZrO_2$, (b) CuO_5 and (c) CuO_4 clusters drawn by VESTA.[10] Black lines are the boundaries of a supercell in (a) and bond lengths (Å) are shown in (b) and (c). Color code: green, Zr; blue, Cu; and red, O.

Fig. 7 shows the optimized structures of the bulk $CuO/t\text{-}ZrO_2$. The Cu atom is penta-coordinated (Fig. 7b) in the lowest-energy structure, in contrast to the four-fold coordination of Cu in CuO and the eight-fold coordination of Zr in $t\text{-}ZrO_2$. However, we also observed a four-fold-coordinated Cu cluster (Fig. 7c) as a metastable structure (energetically slightly higher than 0.04 eV per formula unit). The examined bulk $CuO/t\text{-}ZrO_2$ structures displayed a 1:1 five- to four-fold coordination ratio, indicating that the two species were almost mixed equally in the bulk. Notably, the four-fold-coordinated Cu cluster shown in Fig. 7c is not completely square planar but rather a distorted tetrahedral.

Fig. 8 shows the surface structure of the solid-solution $CuO/t\text{-}ZrO_2$ surface. The coordination number of the surface Cu atom is four, which is less than the five observed in the most stable bulk structure. The Cu–O bond lengths of the $[CuO_4]$ cluster shown in Fig. 8b range from 1.94 to 2.00 Å. The shape of the $[CuO_4]$ cluster is almost square planar, which is different from that of bulk $CuO/t\text{-}ZrO_2$.

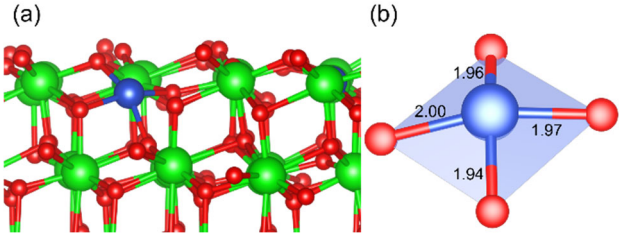

Fig. 8 Side view of the $CuO/t\text{-}ZrO_2$ surface and $[CuO_4]$ cluster. The bond lengths (Å) are shown in (b).

Reaction mechanism.

We next considered the reaction mechanism of Cu-catalyzed Chan-Lam coupling over $CuO/t\text{-}ZrO_2$. One of the important factors here is the positive correlation between the product yields and Cu^{2+} reducibility (Fig. 6). This suggests that the redox cycle of the Cu^{2+} species is essential for Cu-catalyzed Chan-Lam coupling to occur. We therefore adopted a computational approach to further understand the role of the Cu^{2+} species at the molecular level. Fig. 9 shows that the adsorption of both the imidazole and benzene molecules on the surface Cu sites of the $CuO/t\text{-}ZrO_2$ surface is exothermic, with an

This journal is © The Royal Society of Chemistry 20xx

Please do not adjust margins

Please do not adjust margins

adsorption energy of −0.37 eV. When the adsorbates adsorb to the surface Cu atom, the adsorbates transfer protons to the O atoms at the catalyst surface. The adsorbed structure in Fig. 9 exhibits characteristic Cu coordination: The surface Cu atom forms four bonds with C (in benzene), N (in imidazole), and two surface O atoms (in the $[CuO_4]$ cluster) atoms by breaking two Cu–O bonds in the $[CuO_4]$ cluster at the CuO/*t*-ZrO_2 surface. Notably, the surface Cu atom moves away from the surface by 1.54 Å along the surface normal direction upon adsorption. The Cu–O bond lengths were 1.84 Å and 2.16 Å, and their strength was almost the same as that at the CuO/*t*-ZrO_2 surface (Fig. 8). These findings indicate that the imidazole and benzene molecules adsorb onto the Cu active site that detaches from the $[CuO_4]$ cluster. After the product (**3a**) is formed, the Cu atom returns to the $[CuO_4]$ cluster, as shown in Fig. 8.

$E_{ads} = -0.37$ eV

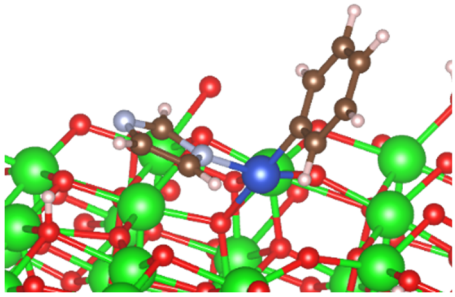

Fig. 9 Adsorption structure of imidazole and benzene molecules at the CuO/*t*-ZrO_2 surface. The adsorption energy (E_{ads}) is also displayed. Color code: green, Zr; blue, Cu; red, O; brown, C; light blue, N; and white, H.

Next, we assumed a reaction mechanism for the Chan-Lam coupling of phenylboronic acid **1a** and imidazole **2a** using the CuO/*t*-ZrO_2 catalyst (Fig. 10).[7b] Initially, transmetalation of **2a** to form the Ph-imidazole-CuO_2 intermediate from $[CuO_4]$. The oxidation of Cu^{2+} to Cu^{3+} occurs by O_2 in air.[11] Subsequent reductive elimination provides the desired product **3a** and Cu^{1+} species. Finally, the initial $[CuO_4]$ species is regenerated through the aerobic oxidation of Cu^{1+}.[12]

Fig. 10 Proposed reaction mechanism

Based on the proposed reaction mechanism, analytical results, and DFT calculations, we assumed that the highly reducible square planar $[CuO_4]$ in CuO/*t*-ZrO_2 exhibited superior performance because of smooth transmetalation from Cu–O bondings to Cu–C and Cu–N bondings. In contrast, the octahedral $[CuO_6]$ in CuO/Al_2O_3 exhibited lower reactivity for Chan-Lam coupling, probably because of the less reducible Cu species. The reactions using CuO/TiO_2 and CuO/*m*-ZrO_2 showed lower reactivities because the Cu species were not doped, but supported on metal oxides.

Substrate scope and recycling catalyst.

Under the optimal reaction conditions listed in Table 1, we next examined the substrate scope (Scheme 1). Chan-Lam coupling of 4- and 3-tolylboronic acids **1b** and **1c** with imidazoles **2** provided the corresponding products **3b** and **3c** in 93% and 99% yields, respectively. Sterically hindered 2-tolylboronic acid **1d** was also tolerated, affording the *N*-arylated imidazole **3d** in 76% yield. When 4-chloro- and 4-methoxyphenylboronic acids **1e** and **1f** were used as substrates, the desired products **3e** and **3f** were obtained in 71% and 77% yields, respectively. 1- and 2-Naphthylboronic acids **1g** and **1h** were successfully converted to the corresponding products **3g** and **3h** in good yields (**3g**: 77%, **3h**: 81%). The reaction using 3-thienylboronic acid as a heterocyclic substrate yielded the product **3i** in 37% yield. Although the cross coupling of **1b** with 2-methyl imidazole **2b** provided the desired product **3j** in 28% yield, benzimidazole **2c** was not a suitable substrate, probably due to steric bulkiness. When we reused CuO/*t*-ZrO_2 catalyst after Chan-Lam coupling of **1a** and **2a**, the yield of **3a** was decreased to 58%.

Scheme 1. Scope of substrates using CuO/*t*-ZrO_2 catalyst[a,b]

[a]Reaction conditions: Reaction was conducted using **1** (0.2 mmol), **2** (0.2 mmol), and the catalyst (0.01 mmol, 5 mol%) in MeOH (1.0 mL, 0.2 M) at 50 °C for 8 h in air. [b]Isolated yield.

Please do not adjust margins

Please do not adjust margins

Conclusions

We demonstrated the efficient Chan-Lam coupling of imidazole and boronic acids when catalyzed by CuO/*t*-ZrO_2. The reaction proceeded smoothly under air atmosphere and mild conditions in the absence of external additives, affording the corresponding *N*-arylated compounds (TON = 15 for the synthesis of **3a**). Of note, the TON of CuO/*t*-ZrO_2 was more than ten times higher than that of CuO nanoparticles. XRD, XAS, and DFT structural analyses characterized the square planar Cu species, [CuO_4], dispersed on the CuO/*t*-ZrO_2 surface. H_2-TPR analyses indicated that the [CuO_4] species are highly reducible, and thus, that they may have good redox properties. DFT calculations also suggested the co-adsorption of imidazole and benzene on the surface of the Cu site, which can be an essential step in Chan-Lam coupling. Notably, similar to ligands for homogeneous catalysts, the types of support materials for heterogeneous catalysts determine the coordination structure of the Cu species: CuO nanoparticles are formed on the TiO_2 and *m*-ZrO_2 surfaces, octahedral [CuO_6] species are formed in Al_2O_3, and [CuO_4] species are selectively formed on the *t*-ZrO_2 surface. This study opens up the possibility that heterogeneous copper catalysts can be applied in organic synthesis reactions. Further catalytic applications of CuO/*t*-ZrO_2 and mechanistic studies are ongoing in our laboratory.

Experimental section

Catalyst preparation

In this study, four types of CuO/MO_x catalysts (MO_x = TiO_2, Al_2O_3, *m*-ZrO_2, and *t*-ZrO_2) were prepared using an incipient wetness impregnation method; Evonik P-25 was used as the TiO_2. Al_2O_3 (JRC-ALO-8) and *m*-ZrO_2 (JRC-ZRO-3) were supplied by the Catalysis Society of Japan, while amorphous ZrO_2 (NND) was provided by Daiichi Kigenso Kagaku Kogyo. First, MO_x was impregnated with an aqueous solution of $Cu(NO_3)_2{\cdot}3H_2O$ (Fujifilm Wako, Japan). The obtained powder was then dried at 110 °C and subsequently the powder was calcined at 500 °C for 3 h. Their CuO contents was 1 mmol g^{-1} and, commercial CuO was used as the reference (Fujifilm Wako, Japan).

Characterization of catalysts

X-ray diffraction (XRD), X-ray fluorescence (XRF), X-ray absorption spectroscopy (XAS), scanning transmission electron microscopy (STEM), and H_2 temperature-programmed reduction (H_2-TPR) were carried out to characterize the as-synthesized catalysts. The detailed procedures are described in the ESI.

Reaction test

Each test-tube was charged with phenylboronic acid **1a** (0.2 mmol, 24.4 mg), imidazole **2a** (0.2 mmol, 13.6 mg) and the catalyst (0.01 mmol Cu) in 1 mL MeOH. The resulting solution was stirred at 50 °C in air. After 8 h, the organic layer was separated with the Cu catalyst and concentrated under reduced pressure. The residue was purified by silica gel column chromatography (hexane:ethyl acetate ratio = 5:5) to obtain the pure product **3a**. TON values were determined by dividing the quantity of **3a** produced after 8 h by the moles of the Cu catalyst.

Density functional theory (DFT) calculations

DFT calculations were performed using the Perdew-Burke-Ernzerhof (PBE)[13] exchange and correlation functional and D3 correction[14] using the cp2k program package,[15] based on the computational procedures reported in our previous work.[16] The Goedecker-Teter-Hutter pseudopotentials[17] and a double-ζ valence plus polarization (DZVP-MOLOPT-SR-GTH)[18] Gaussian basis set for the orbitals were employed. The cutoff associated with mapping Gaussians onto a multi-grid was 60 Ry and the planewave cutoff for the finest level of the multi-grid was 400 Ry. We employed $3 \times 3 \times 4$ Monkhorst-Pack[19] *k*-point meshes and Γ point for the *k*-point samplings of the bulk and surface, respectively. The target accuracy for the SCF (self-consistent field) convergence was 10^{-5}.

DFT calculations of bulk CuO/*t*-ZrO_2

The initial bulk geometry of the supercell was generated using a periodic $2 \times 2 \times 1$ supercell of *t*-ZrO_2.[20] Fermi-Dirac smearing was employed at an electronic temperature of 300 K. To model the solid solution, the Zr and O atoms were replaced with a Cu atom and oxygen vacancy (V_O), respectively, to maintain the neutrality of the system. Bulk CuO/*t*-ZrO_2 was prepared by ZrO_2 with a Cu–V_O pair to afford $Cu_xZr_{1-x}O_{2-x}$ with a molar ratio of x = 1/8 = 0.125. We first replaced an O atom in the supercell (Zr_8O_{16}) with V_O. Using the optimized structure with the lowest energy, we next replaced the Cu atom with a Zr atom to form Zr_7CuO_{15} that has the lowest energy.

DFT calculations of surface CuO/*t*-ZrO_2

The *t*-ZrO_2 (101) surface was generated from the optimized bulk structure. The rectangular slab consisted of $Zr_{40}O_{80}$ and the dimensions of the super cell were 12.702×14.472 Å^2 and 35.000 Å along the surface-parallel and surface-normal directions, respectively. The bottom ZrO_2 layer of the six layers was fixed to the bulk structure, and the geometry of the remaining atoms was optimized. To prepare CuO/*t*-ZrO_2, we replaced two Cu–V_O pairs in the top layer of the zirconia surfaces. The molar ratio of the top two ZrO_2 layers in $Cu_xZr_{1-x}O_{2-x}$ was x = 1/8 = 0.125. The Supporting Information details the computational conditions and results of the formation free energy of the CuO/*t*-ZrO_2 surface,[21] and the atomic charges around the Cu atoms by Hirshfeld analysis[22] using a hybrid functional (PBE + 10.5% Hartree-Fock exchange).[23]

DFT calculations of adsorption energy

The adsorption energy was calculated using the equation.

$$E_{\text{ads}} = E_{\text{substrate+adsorbate}} - E_{\text{substrate}} - E_{\text{adsorbate}}$$

where $E_{\text{substrate+adsorbate}}$, $E_{\text{substrate}}$, and $E_{\text{adsorbate}}$ are the energies of the substrate and adsorbate, substrate, and adsorbate, respectively. The adsorbates were benzene and imidazole molecules to model the reactants of the reaction considered in this study.

Conflicts of interest

There are no conflicts of interest to declare.

Acknowledgements

The authors gratefully acknowledge generous support by JSPS KAKENHI Grant Numbers 21K04988, Research Foundation for JFE 21st Century Foundation. The authors thank the Center for Instrumental Analysis, Ibaraki University, for its help with XRD and XPS. The synchrotron radiation experiments were performed at BL14B2 of SPring-8 with the approval of the Japan Synchrotron Radiation Research Institute (JASRI, Proposal no. 2022A1782). We used the supercomputers of the Institute for Solid State Physics, the University of Tokyo, and the Research Institute for Information Technology, Kyushu University.

 This journal is © The Royal Society of Chemistry 20xx

Please do not adjust margins

Please do not adjust margins

Notes and references

1. For selected reviews on heterogeneous Cu catalysts, see: (*a*) S. D. Senanayake, D. Stacchiola and J. A. Rodriguez, *Acc. Chem. Res.,* 2013, **46**, 1702; (*b*) S. Bordiga, E. Groppo, G. Agostini, J. A. van Bokhoven and C. Lamberti, *Chem. Rev.,* 2013, **113**, 1736; (*c*) M. B. Gawande, A. Goswami, F.-X. Felpin, T. Asefa, X. Huang, R. Silva, X. Zou, R. Zboril and R. S. Varma, *Chem. Rev.,* 2016, **116**, 3722; (*d*) L. Liu and A. Corma, *Chem. Rev.,* 2018, **118**, 4981.
2. For selected reviews on applications of heterogeneous Cu catalyst to organic syntheses, see: (*a*) S. E. Allen, R. R. Walvoord, R. Padilla-Salinas and M. C. Kozlowski, *Chem. Rev.,* 2013, **113**, 6234; (*b*) C. Sambiagio, S. P. Marsden, A. J. Blacker and P. C. McGowan, *Chem. Soc. Rev.,* 2014, **43**, 3525; (*c*) V. K. Tiwari, B. B. Mishra, K. B. Mishra, N. Mishra, A. S. Singh, X. Chen, *Chem. Rev.,* 2016, **116**, 3086; (*d*) S. Bhunia, G. G. Pawar, S. V. Kumar, Y. Jiang and D. Ma, *Angew. Chem., Int. Ed.,* 2017, **56**, 16136; (*e*) N. Aflak, H. Ben El Ayouchia, L. Bahsis, H. Anane, M. Julve and S.-E. Stiriba, *Int. J. Mol. Sci.*, 2022, **23**, 2383; (*f*) R. Zhang, Y. Chen, M. Ding and J. Zhao, *Nano Res.,* 2022, **15**, 2810.
3. (*a*) M. Mafokoane, J. Seguel, R. García, J. N. Díaz de León, C. Sepúlveda and N. Escalona, *Catal. Today,* 2021, **367**, 310; (*b*) Z. Cai, A. Li, W. Zhang, Y. Zhang, L. Cui and J. Liu, *J. Alloy Compd.,* 2021, **882**, 160749.
4. (*a*) T. Liu, L. Wei, Y. Yao, L. Dong and B. Li, *Appl. Surf. Sci.,* 2021, **546**, 148971; (*b*) G. Wang, W. An, Y. Zhang, Z. Liu, S. Yang, P. Jin and D. Ding, *Chem. Eng. J.,* 2022, **430**, 133060; (*c*) Z. Zhang, L. Fan, W. Liao, F. Zhao, C. Tang, J. Zhang, M. Feng and J.-Q. Lu, *J. Catal.,* 2022, **405**, 333.
5. (*a*) A. G. Sato, D. P. Volanti, D. M. Meira, S. Damyanova, E. Longo and J. M. C. Bueno, *J. Catal.,* 2013, **307**, 1; (*b*) T. Witoon, J. Chalorngtham, P. Dumrongbunditkul, M. Chareonpanich and J. Limtrakul, *Chem. Eng. J.,* 2016, **293**, 327. (*c*) I. Ro, Y. F. Liu, M. R. Ball, D. H. K. Jackson, J. P. Chada, C. Sener, T. F. Kuech, R. J. Madon, G. W. Huber and J. A. Dumesic, *ACS Catal.,* 2016, **10**, 7040; (d) G.-Y. Yang, Y.-H. Ke, H.-F. Ren, C.-L. Liu, R.-Z. Yang and W.-S. Dong, *Chem. Eng. J.,* 2016, **283**, 759; (*e*) N. Scotti, F. Bossola, F. Zaccheria and N. Ravasio *Catalysts,* 2020, **10**, 168; (*f*) Y. Shao, T. Wang, K. Sun, Z. Zhang, L. Zhang, Q. Li, S. Zhang, G. Hu and X. Hu, *Green Energy Environ.,* 2021, **6**, 557; (*g*) J. Jiang, L. Du, Y. Ding, *ChemistrySelect,* 2021, **6**, 1372; (*h*) H. Zhao, R. Yu, S. Ma, K. Xu, Y. Chen, K. Jiang, Y. Fang, C. Zhu, X. Liu, Y. Tang, L. Wu, Y. Wu, Q. Jiang, P. He, Z. Liu and L. Tan, *Nat. Cat.,* 2022, **5**, 818.
6. (*a*) S. Tada, A. Katagiri, K. Kiyota, T. Honma, H. Kamei, A. Nariyuki, S. Uchida and S. Satokawa, *J. Phys. Chem. C,* 2018, **122**, 5430; (*b*) S. Tada, S. Kayamori, T. Honma, H. Kamei, A. Nariyuki, K. Kon, T. Toyao, K.-I. Shimizu and S. Satokawa, *ACS Catal.,* 2018, **8**, 7809; (*c*) S. Tada, K. Oshima, Y. Noda, R. Kikuchi, M. Sohmiya, T. Honma and S. Satokawa, *Ind. Eng. Chem. Res.,* 2019, **58**, 19434; (*d*) S. Tada, K. Fujiwara, T. Yamamura, M. Nishijima, S. Uchida and R. Kikuchi, *Chem. Eng. J.,* 2020, **381**, 122750.
7. For selected recent reviews, see: (*a*) I. Munir, A. F. Zahoor, N. Rasool, S. A. R. Naqvi, K. M. Zia and R. Ahmad, *Mol. Divers.,* 2019, **23**, 215; (*b*) M. J. West, J. W. B. Fyfe, J. C. Vantourout and A. J. B. Watson, *Chem. Rev.,* 2019, **119**, 12491; *(c*) J.-Q. Chen, J.-H. Li and Z.-B. Dong, *Adv. Synth. Catal.,* 2020, **362**, 3311; (*d*) R. A. Fernandes, A. Bhowmik and S. S. Yadav, *Org. Biomol. Chem.,* 2020, **18**, 9583.
8. (*a*) P. Halder, T. Roy and P. Das, *Chem. Commun.,* 2021, **57**, 5235; (*b*) S. Ananthu, T. Aneeja and G. Anilkumar, *ChemistrySelect*, 2021, **6**, 9794.
9. (a) T. Yokoyama, N. Kosugi and H. Kuroda, *Chem. Phys.,* 1986, **103**, 101; (*b*) A. Ohta and R. Kubota, *Geostand. Geoanal. Res.,* 2016, **40**, 117.
10. K. Momma and F. Izumi, *J. Appl. Crystallogr*., 2011, **44**, 1272.
11. DFT calculations support the Cu^{3+} species can be present at the CuO/*t*-ZrO_2 surface. For the details, see Fig. S3–S4 in the Supporting Information.
12. Cu^0 species can be generated in Chan-Lam coupling catalyzed Cu complex. However, if metallic Cu^0 forms in our reaction, the catalyst performance can drop. Although long-chain alcohol can be a reductant of CuO/ZrO_2 at elevated temperature (>120 °C) (see ref 5g), methanol did not reduce CuO/*t*-ZrO_2 under our reaction conditions (see Fig. S5).
13. J. P. Perdew, K. Burke and M. Ernzerhof, *Phys. Rev. Lett.,* 1996, **77**, 3865.
14. S. Grimme, J. Antony, S. Ehrlich and H. A. Krieg, *J. Chem. Phys.,* 2010, **132**, 154104.
15. T. D. Kühne, M. Iannuzzi, M. D. Ben, V. V. Rybkin, P. Seewald, F. Stein, T. Laino, R. Z. Khaliullin, O. Schütt, F. Schiffmann, et al. *J. Chem. Phys.,* 2020, **152**, 194103
16. S. Tada, N. Ochiai, H. Kinoshita, M. Yoshida, N. Shimada, T. Joutsuka, M. Nishijima, T. Honma, N. Yamauchi, Y. Kobayashi and K. Iyoki, *ACS Catal.,* 2022, **12**, 7748
17. (*a*) S. Goedecker, M. Teter and J. Hutter, *J. Phys. Rev. B*, 1996, **54**, 1703; (*b*) C. Hartwigsen, S. Goedecker and J. Hutter, *Phys. Rev. B,* 1998, **58**, 3641.
18. J. VandeVondele and J. Hutter, *J. Chem. Phys.,* 2007, **127**, 114105.
19. H. J. Monkhorst, and J. D. Pack, *Phys. Rev. B,* 1976, **13**, 5188.
20. N. Igawa and Y. Ishii, *J. Am. Ceram. Soc.,* 2001, **84**, 1169.
21. (*a*) J. S. Elias, N. Artrith, M. Bugnet, L. Giordano, G. A. Botton, A. M. Kolpak and Y. Shao-Horn, *ACS Catal.,* 2016, **6**, 1675; (*b*) K. Reuter and M. Scheffler, *Phys. Rev. B,* 2001, **65**, 035406.
22. F. L. Hirshfeld, *Theor. Chim. Acta,* 1977, **44**, 129.
23. (*a*) A. R. Elmaslmane, M. B. Watkins and K. P. McKenna, *J. Chem. Theory Comput.,* 2018, **14**, 3740; (*b*) T. Joutsuka, H. Yoshinari, and S. Yamauchi, *Bull. Chem. Soc. Jpn.,* 2021, **94**, 106.

Please do not adjust margins